Ultimate Strength Characteristics of Unstiffened Cylindrical Shell in Axial Compression

Shen Li[1], Do Kyun Kim[2,3]

[1]Department of Naval Architecture, Ocean and Marine Engineering, University of Strathclyde, Glasgow, UK

[2]Department of Naval Architecture and Ocean Engineering, Seoul National University, Seoul, Korea

[3]Research Institute of Marine Systems Engineering, Seoul National University, Seoul, Korea

Corresponding authors: shen.li@strath.ac.uk (Shen Li); do.kim@snu.ac.kr (Do Kyun Kim)

Abstract: Cylindrical shell is a common structural design solution in many engineering fields, such as the foundation supporting structures and buoyant column of the offshore wind turbine in the maritime sector. Operating in an ocean environment, these cylindrical shell structures need to withstand a combination of axial compression, bending moment, torsion and external pressure. This study contributes a parametric investigation for unstiffened cylindrical shells subjected to axial compression. Emphasis is placed on the ultimate strength characteristics and their relation with the initial geometric imperfection. The nonlinear finite element method is adopted by considering geometric and material nonlinearities in conjunction with an arc-length incrementation to solve the governing equilibrium equation. The numerical prediction is compared with the prevailing code-based approach, i.e. DNV, ABS, API and Eurocode. This study shows that the ultimate strength of unstiffened cylindrical shells in axial compression is highly sensitive to initial geometric imperfection. The code-based formulae appear to be overly conservative for predicting the ultimate compressive strength of cylindrical shells.

Highlights

- Numerical collapse test of unstiffened cylindrical shell under axial compression.
- A range of initial imperfection shapes with different deflection modes in longitudinal and circumferential directions are analysed.
- Comparison is completed between the numerical prediction and code formulae.

Keywords: Shell, buckling, ultimate strength, stability, finite element method

Nomenclature

E	Elastic modulus of material
σ_Y	Yield strength of material
ν	Poisson's ratio
t	Shell thickness
l	Length of cylindrical shell
R	Radius of cylindrical shell
D	Diameter of cylindrical shell
x	Longitudinal coordinate
y	Transverse coordinate
z	Transverse coordinate
θ	Polor coordinate
w	Initial geometric deflection
w_{max}	Maximum magnitude of initial geometric deflection
m	Half-wave number of longitudinal deflection
n	Full-wave number of circumferential deflection
Q	Fabrication quality parameter in Eurocode 3

1. Introduction

Many countries have set out their commitments for net-zero emission in the light of addressing the detrimental impact caused by greenhouse gas and the consequent climate change. It is inevitable

that the use of traditional fossil fuels has to be limited in the near future. However, this is often resisted by the demand for industrial development where sufficient energy supply is an important ingredient. Hence, to accelerate the ambitious net-zero target while ensuring a sufficient energy supply, the exploitation of wind energy is one of the sustainable and clean solutions. In fact, the benefits of wind energy are well recognised nowadays, and it is foreseen that the investment in the construction of wind farms will continue in the coming years [1].

Cylindrical shell is a typical solution in designing wind turbine towers and supporting foundations (e.g., monopile and buoyant). Therefore, a thorough integrity assessment using rational evaluation procedures for these structures is of great importance for the wind energy industry [2,3]. Limit state design has been a proven scientific approach for assessing the integrity of different kinds of engineering structures [4,5]. Four limit states are usually relevant, namely Serviceability Limit State (SLS) [6], Fatigue Limit State (FLS) [7,8], Accidental Limit State (ALS) [9] and Ultimate Limit State (ULS) [10,11]. SLS is determined by limiting values that are oriented towards the normally envisaged use of a structural system. FLS refers to the failure due to cumulative damage of repeated loading that leads to the initiation and propagation of cracks and eventually fractures. ALS examines the damage tolerance of structural systems in an accidental event, such as collision, grounding, fire, explosion etc.

The present study focuses on the Ultimate Limit State (ULS), which concerns the maximum load-carrying capacity of the structures and is a typical assessment criterion in the initial design [12-14]. Operating in a marine environment, the cylindrical shell structures need to withstand the environmental loads in the form of axial loads (N_x), overturning bending moment (M_z or M_y), torsion (M_x) and external pressure (p_{hydro} or p_{wind}) (**Figure 1**).

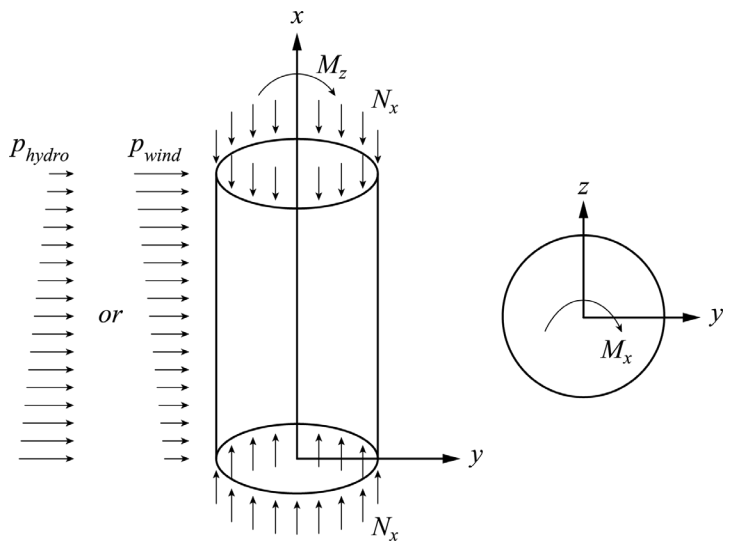

Figure 1. Typical loading profile on cylindrical shell structures

A number of studies are available in the literature reporting the nonlinear structural response cylindrical shell structures. Kim and Kim [15] conducted a parametric numerical study for unstiffened cylindrical shells under axial compression. A design formula was proposed to evaluate the buckling stress of the perfect shell based on the numerical data, and the effects of the different foundations were investigated. Shiomitsu and Yanagihara [16-17] analysed the elastic buckling strength and ultimate capacity of the ring-stiffened shell under external pressure using nonlinear finite element methods. The collapse modes were categorised into shell buckling collapse, torsional buckling collapse, and combined buckling collapse. A new slenderness ratio was proposed, with which a formula to estimate the ultimate strength was developed. Cho et al. [18] proposed an ultimate strength formulation based on test data for the ring-stiffened shell under external pressure considering the interaction between different buckling modes. Graham [19] described a finite element study to predict the nonlinear elastoplastic collapse of ring-stiffened cylinders under hydrostatic loading. It was found that if sufficient detail of scantlings, initial deflection, residual stress and material properties are included in a FE model, the collapse pressure of a ring-framed shell structure can be predicted within 6% discrepancy with respect to experimental measurement. An experimental test was performed by Ghazijahani et al. [20] for externally pressurised cylindrical shells. Fully longitudinal stiffening, partially longitudinal stiffening and local thickening were investigated. Instead of the welded connection, a non-welding solution using structural epoxy adhesive for connecting stiffeners/thickeners with the plain shell was proposed.

Cho et al. [21] reported the ultimate strength tests on intact and damaged ring-stiffened cylinders subjected to external hydrostatic pressure. Ghazijahani and Showkati [22] developed an interaction formula to evaluate the ultimate strength of cylindrical shells under combined bending moment and external pressure. Cerik [23] reported a numerical study on the residual ultimate strength of ring-stiffened and orthogonally stiffened damaged cylindrical shells under axial compression. Eigenvalue analysis was adopted to determine the initial imperfection shape, while the imperfection magnitude was determined based on measurements. It was indicated that the dent depth and the flattening around the circumference are the significant parameters in the residual capacity. In addition, it appears that the orthogonally stiffened shell is more damage tolerant than the ring-stiffened shell. Ghazijahani et al. [24] conducted an experimental investigation on cylindrical shells emphasising the effects of local dent imperfection. It was recommended that further research is still required to improve the understanding of various forms of imperfections, particularly localised large dents under different load and boundary conditions. Weaver [25] derived approximate expressions of the shape efficiency for tube sections made of composite material under axial compression. Bo et al. [26] carried out experimental and numerical studies on the buckling of the quasi-perfect shell under axial compression. An integrally manufactured cylindrical shell was adopted to isolate the fabricated-induced imperfection. It serves as a benchmark for investigating the effect of geometric imperfections on the buckling behaviour of the cylindrical shell. Schmidt and Winterstetter [27] carried out experimental and numerical investigations on the buckling behaviour of unstiffened cylindrical shells loaded by combined axial compression and torsion. Pal'chevskii [28] showed that the buckling mode of the cylindrical shell under axial compression (number of half-wave in the circumferential direction n) depends on the ratios L/R and R/t where L, R and t are the length, radius and thickness of the shell. Cho et al. [29] developed an empirical formula to predict the collapse strength of composite cylindrical-shell structures under external pressure loads.

It can be suggested from the literature survey that, in the maritime sector, the research on cylindrical shells usually focuses on their response under external pressure. This is mainly driven by the design of submarines and deep water vehicles. More research efforts and insights are desired to investigate the structural response of cylindrical shells under other loading profiles.

The scope of this paper confines the structural response of cylindrical shells under axial compression, in which case the ultimate failure may be caused by elastic buckling, elastoplastic buckling or gross yielding. In fact, this investigation would also have an impact on understanding the structural behaviour under global bending, where the ultimate collapse is triggered by buckling in the compressed side and the design of ring-stiffened cylindrical shell assuming an inter-frame failure. Different initial imperfection shapes will be analysed to examine the uncertainty propagated to the numerical prediction of ultimate strength. In terms of structural configuration, various combinations of length-to-radius ratios and radius-to-thickness ratios are investigated. The remainder of this paper is organised as follows. Section 2 reviews the prevailing guidance issued by standardisation authorities for cylindrical shells' ultimate limit state analysis. Section 3 provides the principal characteristics of a cylindrical shell and the modelling of initial geometric imperfection. Meanwhile, the test matrix of parametric study is defined. Section 4 introduces the finite element modelling techniques, and Section 5 details the analysis results and insights. Section 6 compares the numerical prediction with prevailing code formulae. Conclusions drawn from this study and recommendations for future research are summarised in Section 7.

2. Background

This section reviews the prevailing code-based approach in the maritime sector for assessing the ultimate limit state of unstiffened cylindrical shell structures (i.e., DNV, ABS, API and Eurocode 3). These formulae are usually employed for the initial assessment of the structural adequacy in terms of the ultimate limit state, with which the principal dimension of a cylindrical structure can be determined. As summarised in the following sections, all these formulae are an adaptation of the classical buckling strength formula of the cylindrical shell. Different knock-down factors are proposed to account for the discrepancy between the classical prediction and experimental measurements. Note that the experimental measurements utilised by different codes for calibration might be different and are not reported in the open literature. The notations of different parameters follow the convention of the each design codes, while some common variables shall refer to the nomenclature.

2.1 DNV Guidance

2.1.1 Limit State Definition (DNV)

According to the recommended practice (DNVGL-RP-C202) issued by DNV (Det Norske Veritas) [30], the buckling strength criterion is given as follows:

$$\sigma_{j,Sd} \leq f_{ksd} \tag{1}$$

where

$\sigma_{j,Sd}$ = Design equivalent von Mises stress

f_{ksd} = Design buckling strength

The design buckling strength (f_{ksd}) is defined as:

$$f_{ksd} = f_{ks}/\gamma_M \tag{2}$$

where γ_M is the material factor and is given as:

γ_M = 1.15 for $\bar{\lambda}_S < 0.5$

γ_M = $0.85 + 0.60\bar{\lambda}_S$ for $0.5 \leq \bar{\lambda}_S \leq 1.0$

γ_M = 1.45 for $\bar{\lambda}_S > 1.0$

The characteristic buckling strength of shells is defined as:

$$f_{ks} = f_y/\sqrt{1 + \bar{\lambda}_S^4} \tag{3}$$

where

f_y = Material yield strength

$\bar{\lambda}_S^2$ = $\frac{f_y}{\sigma_{j,Sd}}\left(\frac{\sigma_{a0,Sd}}{f_{Ea}} + \frac{\sigma_{m0,Sd}}{f_{Em}} + \frac{\sigma_{h0,Sd}}{f_{Eh}} + \frac{\tau_{Sd}}{f_{E\tau}}\right)$

$$\sigma_{j,Sd} = \sqrt{\left(\sigma_{a,Sd}+\sigma_{m,Sd}\right)^2 - \left(\sigma_{a,Sd}+\sigma_{m,Sd}\right)\sigma_{h,Sd} + \sigma_{h,Sd}^2 + 3\tau_{Sd}^2}$$

$$\sigma_{a0,Sd} = \begin{cases} 0, & \sigma_{a,Sd} \geq 0 \\ -\sigma_{a,Sd}, & \sigma_{a,Sd} < 0 \end{cases}$$

$$\sigma_{m0,Sd} = \begin{cases} 0, & \sigma_{m,Sd} \geq 0 \\ -\sigma_{m,Sd}, & \sigma_{m,Sd} < 0 \end{cases}$$

$$\sigma_{h0,Sd} = \begin{cases} 0, & \sigma_{h,Sd} \geq 0 \\ -\sigma_{h,Sd}, & \sigma_{h,Sd} < 0 \end{cases}$$

$\sigma_{a,Sd}$ = Design longitudinal stress due to axial force (positive in tension)

$\sigma_{m,Sd}$ = Design longitudinal stress due to global bending moment (positive in tension)

$\sigma_{h,Sd}$ = Design membrane stress in a circumferential direction

τ_{Sd} = Design shear stress tangential to the shell surface

f_{Ea}, f_{Em}, f_{Eh} and $f_{E\tau}$ are the elastic buckling strength of cylindrical shells subjected to axial compression, global bending moment, lateral pressure and torsional moments and/or shear force, respectively.

2.1.2 Characteristic/Critical Buckling Strength (DNV)

In DNV's guidance, the critical buckling strength of axial compression and global bending moment is given as follows:

$$f_E = C\frac{\pi^2 E}{12(1-\nu^2)}\left(\frac{t}{l}\right)^2 \tag{4}$$

The reduced buckling coefficient may be calculated as:

$$C = \psi\sqrt{1+\left(\frac{\rho\xi}{\psi}\right)^2} \tag{5}$$

The values for ψ, ξ and ρ are summarised in **Table 1**, in which the curvature parameter Z_l is defined by Equation (6). It can be noted from **Table 1** that the coefficient values vary between the axial compression and global bending moment.

$$Z_l = \frac{l^2}{Rt}\sqrt{1-\nu^2} \tag{6}$$

Table 1. Buckling coefficients for unstiffened cylindrical shells

	ψ	ξ	ρ
Axial compression	1.0	$0.702Z_l$	$0.5\left(1+\frac{R}{150t}\right)^{-0.5}$
Global bending moment	1.0	$0.702Z_l$	$0.5\left(1+\frac{R}{300t}\right)^{-0.5}$

2.2 ABS Guidance

2.2.1 Limit State Definition (ABS)

According to the guidance for buckling and ultimate strength assessment for offshore structures (LRFD version) issued by ABS (American Bureau of Shipping) **[31]**, the buckling limit state of unstiffened or ring-stiffened cylindrical shells between adjacent ring stiffeners subjected to axial compression, bending moment and external pressure is to be satisfied the following criterion:

$$\left(\frac{\sigma_x}{\Psi\,\sigma_{CxR}/\gamma_R}\right)^2 - \varphi_R\left(\frac{\sigma_x}{\Psi\,\sigma_{CxR}/\gamma_R}\right)\left(\frac{\sigma_\theta}{\Psi\,\sigma_{C\theta R}/\gamma_R}\right) + \left(\frac{\sigma_\theta}{\Psi\,\sigma_{C\theta R}/\gamma_R}\right)^2 \le 1 \tag{7}$$

where

σ_x = Compressive stress in the longitudinal direction due to factored loads

σ_θ = Compressive hoop stress due to factored loads

σ_{CxR} = Critical buckling stress for axial compression or global bending moment

$\sigma_{C\theta R}$ = Critical buckling stress for external pressure

φ_R = Coefficient to reflect the interaction between longitudinal and hoop stress

$= \frac{\sigma_{CxR} + \sigma_{C\theta R}}{\sigma_Y} - 1.0$

σ_Y = Material yield stress

γ_R = Resistance factor, to be taken as 1.05 unless otherwise specified

Ψ = Maximum allowable strength adjustment factor of shell buckling

= 0.833 if $\sigma_{Cij} \leq 0.55\sigma_Y$

= $0.629 + 0.371\,\sigma_{Cij}/\sigma_Y$ if $\sigma_{Cij} > 0.55\sigma_Y$

σ_{Cij} = Critical buckling stress, e.g., σ_{CxR} and $\sigma_{C\theta R}$ etc.

2.2.2 Characteristic/Critical Buckling Strength (ABS)

The critical buckling strength of unstiffened or ring-stiffened cylindrical shell subjected to axial compression or bending moment may be taken as (Note: there is no difference between the critical buckling strength under axial compression and bending moment in ABS code):

$$\sigma_{CxR} = \sigma_{ExR} \quad \text{for } \sigma_{ExR} \leq P_r\sigma_Y \tag{8a}$$

$$\sigma_{CxR} = \sigma_0\left[1 - P_r(1 - P_r)\frac{\sigma_Y}{\sigma_{ExR}}\right] \quad \text{for } \sigma_{ExR} > P_r\sigma_Y \tag{8b}$$

where

P_r = Proportional linear elastic limit of the structure, to be taken as 0.6 for steel

σ_{ExR} = Elastic compressive buckling stress for an imperfect cylindrical shell

= $\rho_{xR} C \sigma_{CExR}$

σ_{CExR} = Classical compressive buckling stress for a perfect cylindrical shell

= $0.605\frac{Et}{R}$

C = Length dependent coefficient

= 1.0 for $Z \geq 2.85$

= $1.425/Z + 0.175Z$ for $Z < 2.85$

ρ_{xR} = Nominal or lower-bound knock-down factor to allow for shape imperfections

= $0.75 + 0.003z\left(1 - \frac{R}{300t}\right)$ for $Z < 1$

$$= \quad 0.75 - 0.142(Z-1)^{0.4} + 0.003z\left(1 - \frac{R}{300t}\right) \quad \text{for } 1 \le Z < 20$$

$$= \quad 0.35 - 0.0002\frac{r}{t} \quad \text{for } Z \ge 20$$

Z = Batdorf parameter

$$= \quad \frac{l^2}{Rt}\sqrt{1-\nu^2}$$

2.3 API Guidance

2.3.1 Limit State Definition (API)

The bulletin on stability design of cylindrical shells developed by API (American Petroleum Institute) defines the following buckling limit state (Note: $j = l$ for unstiffened cylindrical shell) [32]:

$$\left(\frac{\sigma_{\phi xj}}{\sigma_{xcj}}\right)^2 - c\left(\frac{\sigma_{\phi xj}}{\sigma_{xcj}}\right)\left(\frac{\sigma_{\theta xj}}{\sigma_{rcj}}\right) + \left(\frac{\sigma_{\theta xj}}{\sigma_{rcj}}\right)^2 \le 1 \tag{9}$$

where

$$c \quad = \quad \frac{F_{xcj} + F_{rcj}}{F_y} - 1.0$$

σ_{xcj} = Buckling strength for unstiffened cylindrical shell under compression or bending

σ_{rcj} = Buckling strength for unstiffened cylindrical shell under external pressure

It can be noted that no partial safety factor is applied in the limit state equation defined by API. But according to the API/section 7/stiffener requirement, a design buckling strength may be defined taking into account the safety factor, which equals 1.0 for local buckling and 1.2 for bay instability or general instability. In the present paper, the latter specification is assumed.

2.3.2 Characteristic/Critical Buckling Strength (API)

The buckling strength for cylinders subjected to axial compression or global bending moment are assumed to be the same and given as follows:

$$\sigma_{cL} = \eta\sigma_{eL} \quad \text{for } \sigma_{eL} > 0.5\sigma_Y \tag{9a}$$

$$\sigma_{cL} = \sigma_{eL} \quad \text{for } \sigma_{eL} \leq 0.5\sigma_Y \tag{9b}$$

where

$$\eta = \frac{\sigma_Y}{\sigma_{eL}}\left[\frac{1.0}{1.0 + 3.75(\sigma_Y/\sigma_{eL})^2}\right]^{0.25}$$

$$\sigma_{eL} = C_{xL}\frac{\pi^2 E}{12(1-\nu^2)}\left(\frac{t}{l}\right)^2$$

C_{xL} = Buckling coefficient

$$= \left[1 + \left(\frac{150}{D/t}\right)(\alpha_{xL})^2(M_x^4)\right]^{0.5}$$

α_{xL} = Imperfection factor

$$= 9.0/(300 + D/t)^{0.4}$$

$$M_x = l/(Rt)^{0.5}$$

2.4 Eurocode 3

2.4.1 Limit State Definition (Eurocode 3)

According to Eurocode 3 **[33]**, the buckling limit state of a cylindrical shell is given as:

$$\left(\frac{\sigma_{x,Ed}}{\sigma_{x,Rd}}\right)^{k_x} - k_i\left(\frac{\sigma_{x,Ed}}{\sigma_{x,Rd}}\right)\left(\frac{\sigma_{\theta,Ed}}{\sigma_{\theta,Rd}}\right) + \left(\frac{\sigma_{\theta,Ed}}{\sigma_{\theta,Rd}}\right)^{k_\theta} + \left(\frac{\tau_{x\theta,Ed}}{\tau_{x\theta,Rd}}\right)^{k_\tau} \leq 1 \tag{10}$$

where

$\sigma_{x,Ed}$ = Design longitudinal compressive stress

$\sigma_{\theta,Ed}$ = Design hoop compressive stress

$\tau_{x\theta,Ed}$ = Design shear membrane stress

$\sigma_{x,Rd}$ = Design compressive buckling strength

$\sigma_{\theta,Rd}$ = Design hoop compressive buckling strength

$\tau_{x\theta,Rd}$ = Design shear buckling strength

The exponents k_x, k_θ, k_τ and coefficient k_i are given in terms of the buckling reduction factor (i.e., χ_x, χ_θ and χ_τ) as follows:

$$k_x = 1.0 + \chi_x^2 \quad (11a)$$

$$k_\theta = 1.0 + \chi_\theta^2 \quad (11b)$$

$$k_\tau = 1.0 + \chi_\tau^2 \quad (11c)$$

$$k_i = (\chi_x \chi_\theta)^2 \quad (11d)$$

The buckling reduction factors should be determined as a function of the relative slenderness of the shell ($\bar{\lambda}$):

$$\chi = 1.0 \quad \text{for } \bar{\lambda} \le \bar{\lambda}_0 \quad (12a)$$

$$\chi = 1.0 - \beta\left(\frac{\bar{\lambda} - \bar{\lambda}_0}{\bar{\lambda}_p - \bar{\lambda}_0}\right)^\eta \quad \text{for } \bar{\lambda}_0 < \bar{\lambda} < \bar{\lambda}_p \quad (12b)$$

$$\chi = \frac{\alpha}{\bar{\lambda}^2} \quad \text{for } \bar{\lambda} \ge \bar{\lambda}_p \quad (12c)$$

where

α = Elastic imperfection reduction factor

$$= \frac{0.62}{1 + 1.91(\Delta w/t)^{1.44}} \quad \text{(Compressive elastic imperfection reduction factor)}$$

Δw = Characteristic imperfection magnitude

$$= \frac{1}{Q}\sqrt{\frac{R}{t}}t$$

Q = Fabrication quality parameter, to be taken from **Table 2**

β = Plastic range factor

= 0.60

η = Interaction exponent

= 1.0

$\bar{\lambda}_0$ = Squash limit relative slenderness

= 0.2 (Compressive squash limit relative slenderness)

$\bar{\lambda}_p$ = Plastic limit relative slenderness

= $\sqrt{\frac{\alpha}{1-\beta}}$

$\bar{\lambda}_x$ = Relative shell slenderness parameter for compressive stress

= $\sqrt{f_{yk}/\sigma_{x,Rcr}}$

$\sigma_{x,Ed}$ = $\sigma_{x,Rk}/\gamma_{M1}$

$\sigma_{x,Rk}$ = Characteristic buckling stress

= $\chi_x f_{yk}$

γ_{M1} = Not smaller than 1.1

Table 2. Values of fabrication quality parameter Q

Fabrication tolerance quality class	Description	Q
Class A	Excellent	40
Class B	High	25
Class C	Normal	16

2.4.2 Characteristic/Critical Buckling Strength (Eurocode 3)

In Eurocode 3, the elastic critical buckling strength of unstiffened cylindrical shell under axial compression is given as follows:

$$\sigma_{x,Rcr} = 0.605 E C_x \frac{t}{R} \tag{13}$$

where

C_x = Reduction factor

= 1.0 for medium-length cylinders $1.7 \leq \omega \leq 0.5\frac{R}{t}$

= $1.36 - \frac{1.83}{\omega} + \frac{2.07}{\omega^2}$ for short cylinders $\omega < 1.7$

= $max\left[1 + \frac{0.2}{C_{xb}}\left(1 - 2\omega\frac{t}{R}\right), 0.60\right]$ for long cylinders $\omega > 0.5\frac{R}{t}$

C_{xb} = Parameter dependent on the boundary conditions, to be taken from **Table 3**

ω = Dimensionless length parameter

= $\frac{l}{\sqrt{Rt}}$

Table 3. Parameter C_{xb} for the effect of boundary condition

Case	Cylinder end	Boundary condition	C_{xb}
1	End 1 End 2	BC 1 BC 1	6
2	End 1 End 2	BC 1 BC 2	3
3	End 1 End 2	BC 2 BC 2	1

Note: BC1 = Clamped support; BC2 = Simple support

3. Parametric Study

3.1 Coordinate System

It might be more convenient to adopt a hybrid Cartesian and Polar coordinate system to describe a cylindrical shell structure. As illustrated in **Figure 2**, any position within the cylindrical shell is expressed by combining longitudinal coordinate (x) and angular coordinate (θ). Note that the shell thickness is ignored when defining the coordinate system since the radius is usually overwhelmingly larger than the shell thickness.

For each section along the longitudinal direction, the Polar coordinate system can be transformed into the Cartesian system as follows:

$$y = Rcos(\theta) \tag{14}$$

$$z = Rsin(\theta) \tag{15}$$

This transformation is needed when implementing the geometric imperfection in a finite element model since the nodal coordinate is generally defined by the Cartesian system.

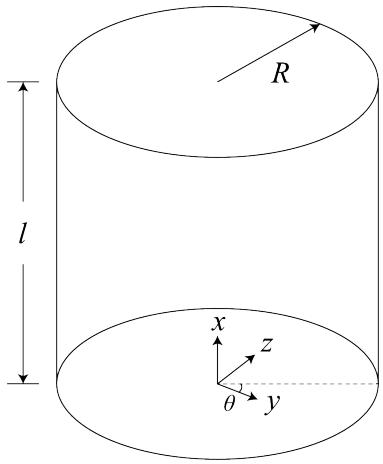

Figure 2. Coordinate system

3.2 Geometric Imperfection

The initial geometric imperfection of a cylindrical shell (unstiffened or ring-stiffened) may be written as the following expression:

$$w(x,\theta) = w_{max} sin\left(\frac{m\pi x}{l}\right) sin(n\theta) \tag{16}$$

where

w_{max} = Maximum imperfection magnitude

l = Length of the unstiffened shell or spacing between ring stiffeners

m = Number of half-wave in the longitudinal direction

n = Number of full-wave in the circumferential direction

In the application of geometric imperfection to the finite element model, Equation (16) is utilised in combination with Equation (14) and (15). Examplar illustrations of the different number of half-

wave in the longitudinal direction and full-wave in the circumferential direction are shown in **Figure 3** and **Figure 4**, respectively.

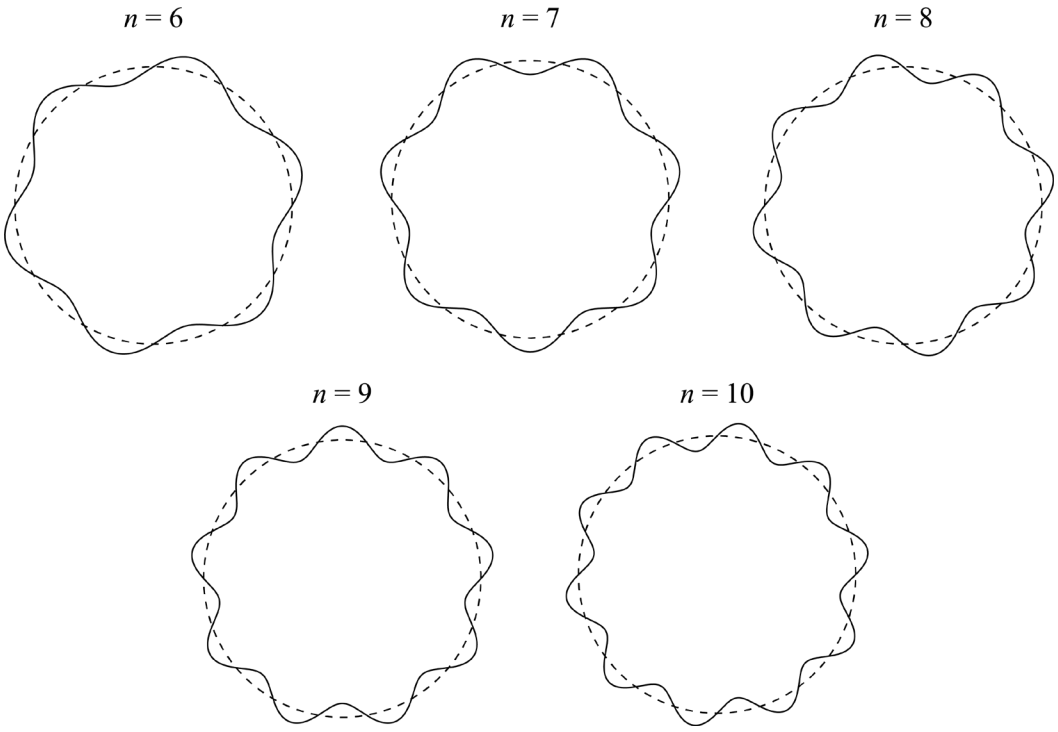

Figure 3. Schematic illustration of geometric imperfection in circumferential direction with different full-wave numbers

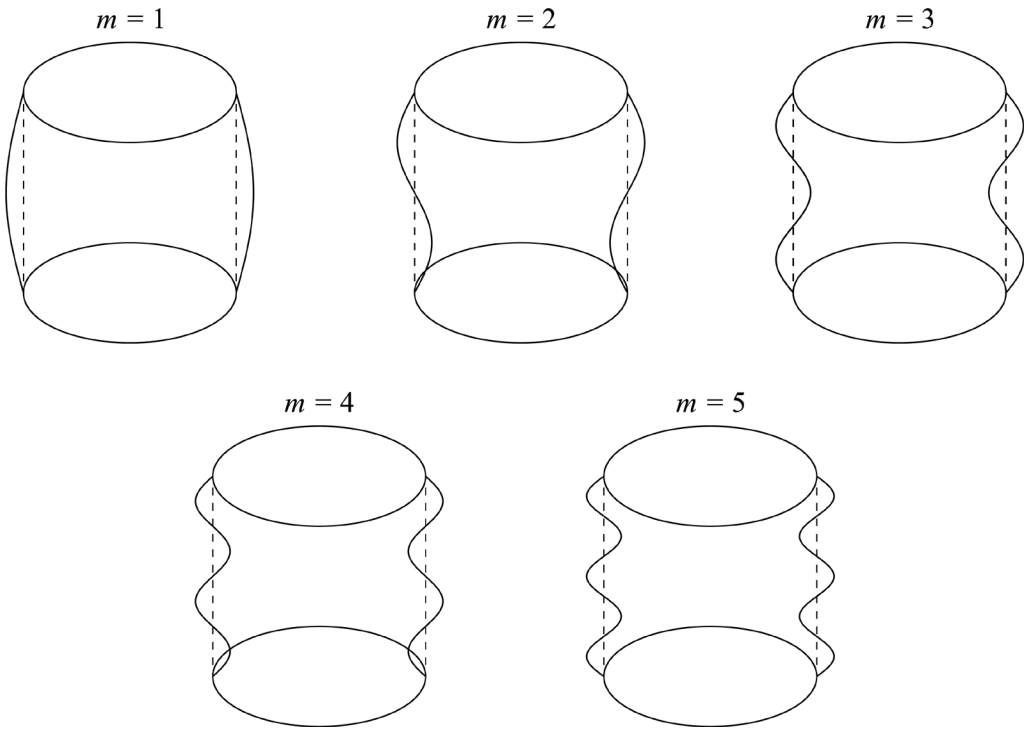

Figure 4. Schematic illustration of geometric imperfection in longitudinal direction with different half-wave numbers

3.3 Test Matrix

The overall test matrix is composed of one hundred (100) primary test cases and five (5) additional test cases. In the primary test matrix, the following features are systematically varied, giving a total of 2 × 2 = 4 cylindrical shell models and 4 × 5 × 5 = 100 test cases:

- Length-to-radius ratio: L/R = 1.0 & 0.4;
- Radius-to-thickness ratio: R/t = 50 & 400;
- Maximum geometric imperfection magnitude: $w_{max}/t = 0.025\left(-2.8+\sqrt{\frac{R}{t}}\right)$ **[34]**;
- Material property: the yield strength and elastic modulus in all calculations are 355 MPa and 207 GPa, respectively;
- Number of half-wave in longitudinal direction: m = 1, 2, 3, 4, 5;
- Number of full-wave in circumferential direction: n = 6, 7, 8, 9, 10;

The objective of the primary test matrix is to investigate the influence of initial geometric imperfection shape on the ultimate strength characteristics of cylindrical shells under axial

compression. The four models represent long & stocky cylindrical shells (L/R = 1.0 & R/t = 50), long & slender cylindrical shell (L/R = 1.0 & R/t = 400), short & stocky cylindrical shell (L/R = 0.4 & R/t = 50), and short & slender cylindrical shell (L/R = 0.4 & R/t = 400). Note that the radius of the cylindrical shell (R) remains constant as 5000 mm throughout the whole test matrix, while the other features are parametrically varied according to the above specification. A summary of the structural configuration and material property is given in **Table 4**.

Table 4. Summary of cylindrical shell models

No.	L [mm]	R [mm]	t [mm]	L/R	R/t	σ_Y [MPa]	E [GPa]
1	5,000	5,000	100	1.0	50	355	207
2	5,000	5,000	12.5	1.0	400	355	207
3	2,000	5,000	100	0.4	50	355	207
4	2,000	5,000	12.5	0.4	400	355	207

The numbers of deflection half-wave in the longitudinal direction and deflection full-wave in the circumferential direction are parametrically varied in the range enclosing the first-order buckling mode shape based on linear eigenvalue analysis. As summarised in **Table 5**, the half-wave number of longitudinal deflection is generally in the range of 1 to 4 (Note: with one exception). The full-wave number of circumferential deflection is typically in the range of 6 to 10 (Note: with one exception). Based on these preliminary results, the longitudinal half-wave and circumferential full-wave variations are specified as 1 to 5 and 6 to 10, respectively. It may be noticed from **Table 5** that the long and slender cylindrical shell model (L/R = 1.0 & R/t = 400) is an outlier with 11 deflection half-waves in the longitudinal direction and 0 deflection full-wave in the circumferential direction, implying a so-called rotational-symmetric imperfection shape. For this reason, an additional test matrix consisting of 5 cases will be completed for this model to analyse the effect of symmetric-rotation imperfection shape. The half-wave number in longitudinal direction $m = 9, 10, 11, 12, 13$.

Table 5. First-order buckling mode shape based on linear eigenvalue analysis

Model	m	n
L/R = 1.0 & R/t = 50	3	6
L/R = 1.0 & R/t = 400	11	0
L/R = 0.4 & R/t = 50	1	6
L/R = 0.4 & R/t = 400	4	10

4. Finite Element Modelling

The finite element model is developed using a four-node shell element with reduced integration, which is a proven element type suitable for buckling analysis of thin-walled structures. The initial geometric imperfection is applied to the finite element model via a direct-node translation approach. A few examples of the finite element model with imperfection are shown in **Figure 5**.

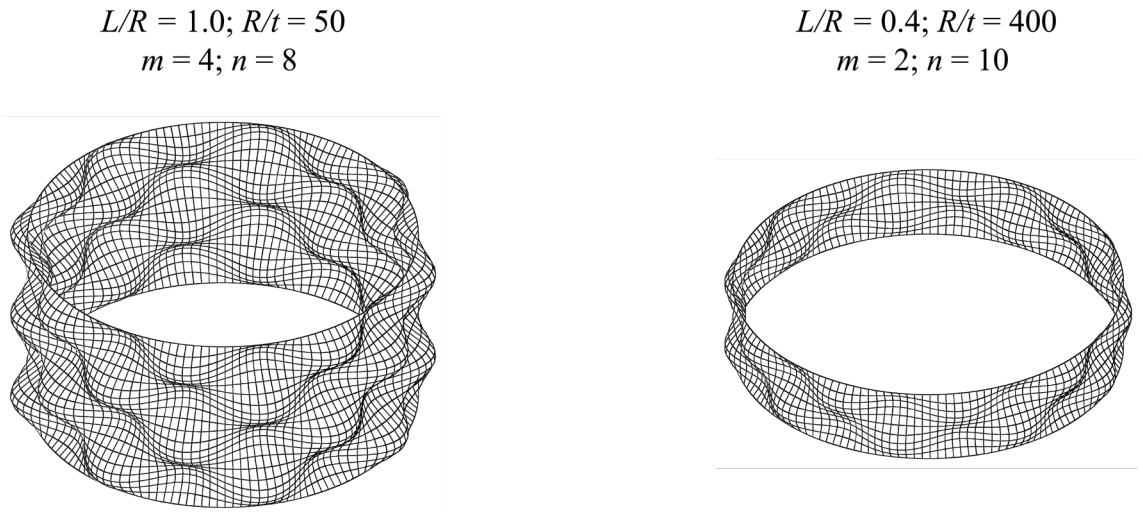

Figure 5. Illustrations of finite element models with geometric imperfection (amplification factor = 50)

As shown in **Figure 6**, the three translational displacements (U_x, U_y, U_z) are constrained at one end of the model, while the two translational displacements (U_y, U_z) are constrained at the opposite end. In the meantime, longitudinal displacement is applied to the model end where longitudinal displacement (U_x) is free. All rotational displacements are set to be free, implying that simply supported boundary is assumed. Note that the axial load is applied through reference points that are coupled to the corresponding model ends. This keeps the loaded edge straight (i.e., uniform displacement) throughout the entire progressive collapse process and allows for more efficient data post-processing.

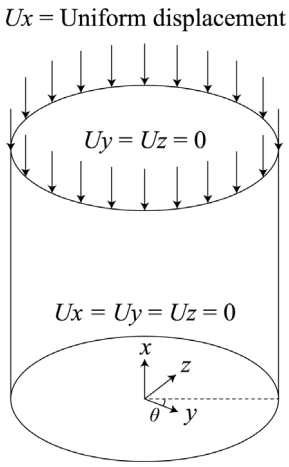

Figure 6. Illustration of boundary condition and loading condition

In terms of the element size, a mesh convergence study is performed. Two cases are selected from the overall test matrix for mesh convergence study:

- $L/R = 1.0$, $R/t = 50$, $w_{max}/t = 0.025\left(-2.8 + \sqrt{\frac{R}{t}}\right)$, $m = 4$, $n = 8$;
- $L/R = 0.4$, $R/t = 400$, $w_{max}/t = 0.025\left(-2.8 + \sqrt{\frac{R}{t}}\right)$, $m = 2$, $n = 10$;

Different mesh densities are considered, with characteristic element sizes ranging from 50mm × 50mm to 300mm × 300mm. As shown in **Figure 7**, the variation in characteristic mesh size does not result in a significant change in the predicted ultimate strength of stocky cylindrical shell with $L/R = 1.0$ and $R/t = 50$. Conversely, a finer mesh leads to a smaller ultimate strength prediction of slender cylindrical shell with $L/R = 0.4$ and $R/t = 400$. It starts to converge when the characteristic mesh size is equal to 100mm × 100mm. In the light of achieving reliable numerical prediction and reducing the computational cost, the mesh size 100mm × 100mm will be adopted for the remaining analyses of this study.

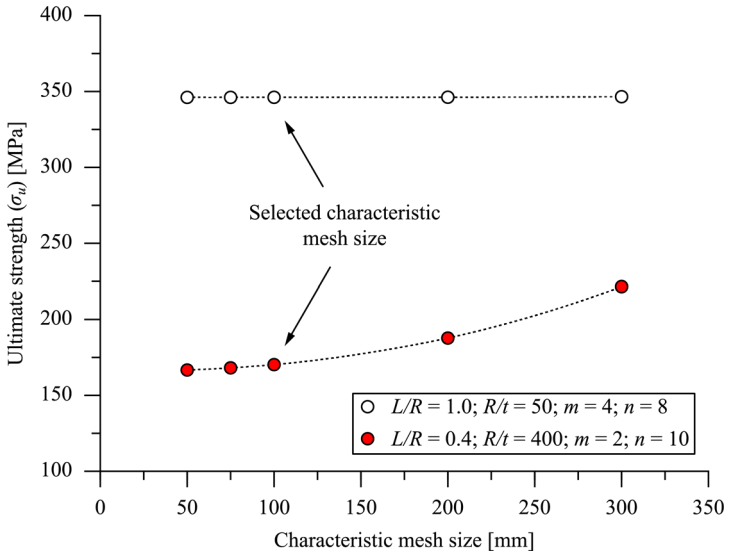

Figure 7. Results of the mesh convergence study

5. Results and Discussions

5.1 Progressive Collapse Behaviour

The progressive collapse behaviour of cylindrical shells under axial compression may be represented by a load-shortening curve (LSC), as shown in **Figure 8**. Two LSCs are illustrated for each case study model, corresponding to the initial imperfection shape that leads to maximum and minimum ultimate strength, respectively. Additionally, the von Mises stress distributions and deflection modes of each model at the ultimate limit state are shown in **Figure 9**.

Similar load-shortening responses are found between finite element models of stocky cylindrical shell models based on different initial imperfection patterns. High ultimate strength is accompanied by a stiff initial response, and the post-collapse unloading is fairly gentle. On the contrary, when it comes to slender cylindrical shell models, steeper post-collapse unloading is shown and in some cases accompanied with a significant snap-back response.

The present study is confined to the unstiffened cylindrical shell structures. Generally, the primary collapse mode of stocky shells is material yielding, whereas the primary collapse mode of slender shells is buckling accompanied by yielding. Thus, the collapse modes are shell buckling and yielding. Nevertheless, this is also greatly affected by the initial geometric imperfection shape.

For instance, if a lower-order longitudinal deflection is assumed in the stocky shells (e.g., $m = 1$), while following the initial pattern, the out-of-circulation deflection hardly developed. Yielding initiates at two edges of the models and propagate toward the central shell, which appears to be the primary cause of the collapse.

On the contrary, if a higher-order longitudinal deflection, e.g., $m = 5$ for model with $L/R = 1.0$ & $R/t = 50$, an appreciable out-of-circulation deflection will be developed consistent with the initial profile (**Figure 10a**). This is accompanied with yielding initiated in the outward-deflected wave, and the collapse in this case shall be considered as the combined resultant of buckling and yielding.

In principle, the above behaviour can also be found in short cylindrical shells (both stocky and slender). The exception, however, is the collapse behaviour of long and slender shell model, i.e., $L/R = 1.0$ & $R/t = 400$. In this scenario, the development of the wavy circumferential deflection seems to be affected by the rotational-symmetric pattern, which is the preferred buckling mode according to the linear buckling analysis. At the collapse state, it appears that all the crest and trough resume to the perfect position. In contrast, an outward-deflected wave is developed at the initially zero-crossing position (**Figure 10b**). In terms of the longitudinal deflection, when assuming lower-order initial deflection mode, it develops in a similar way as the stocky counterpart, and localisation on two edges is observed. This localisation is accompanied by yielding initiation and propagation toward the central shell. If a higher-order longitudinal deflection is assumed, it follows the initial pattern in the initial phase of the loading application. A considerable localisation of deflection occurs at the central shell when approaching the limit state. Note that no yielding occurs in this case, and the collapse is entirely triggered by elastic buckling.

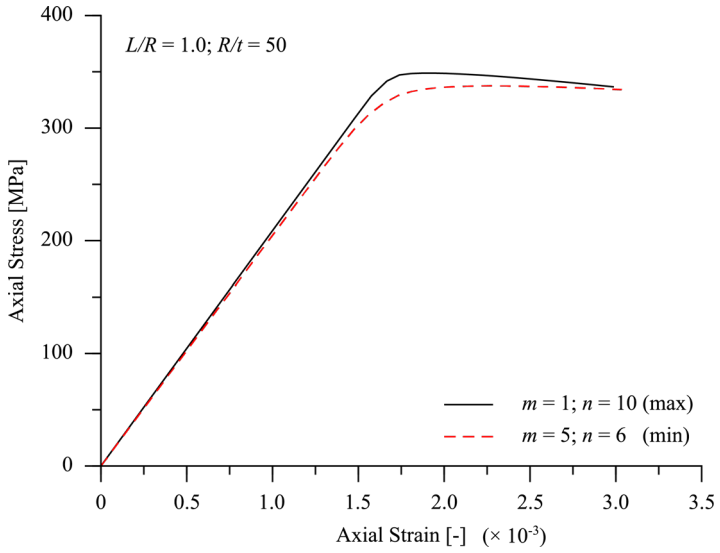

Figure 8(a). The load-shortening curve of long stocky cylindrical shell

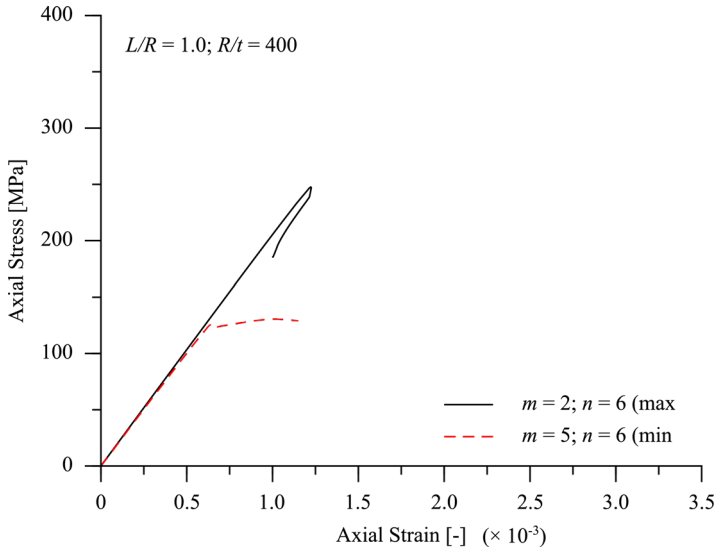

Figure 8(b). The load-shortening curve of long slender cylindrical shell

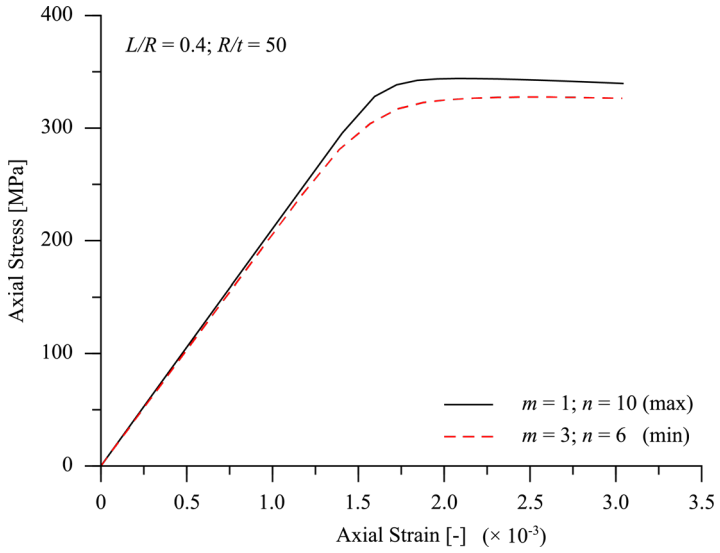

Figure 8(c). The load-shortening curve of short stocky cylindrical shell

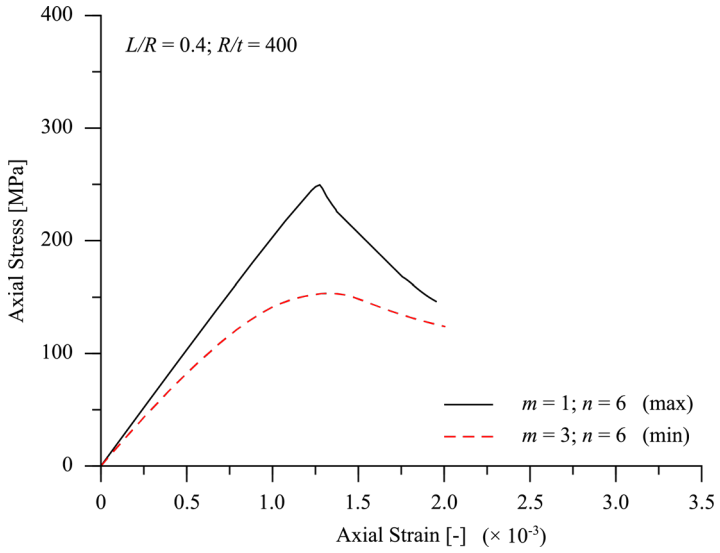

Figure 8(d). The load-shortening curve of short slender cylindrical shell

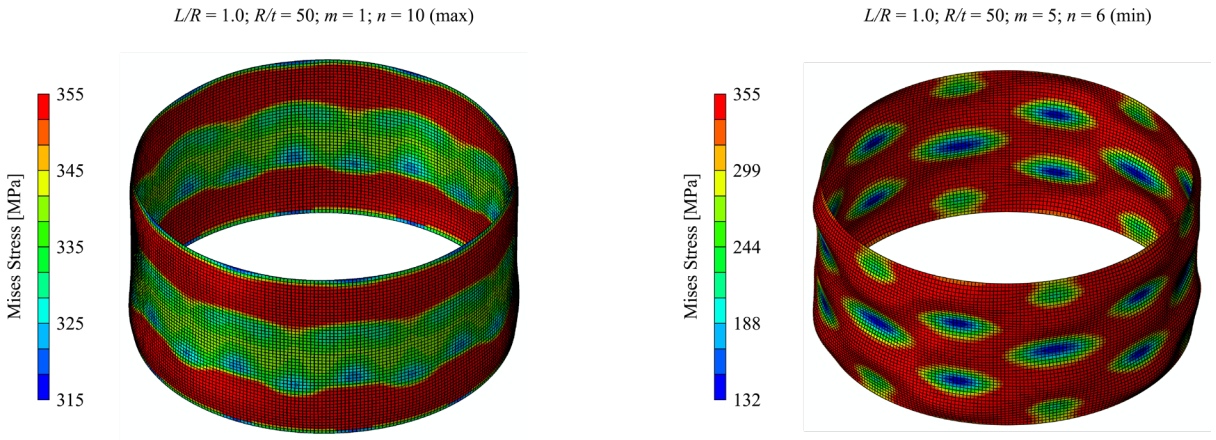

Figure 9(a). Typical collapse modes of long stocky cylindrical shell

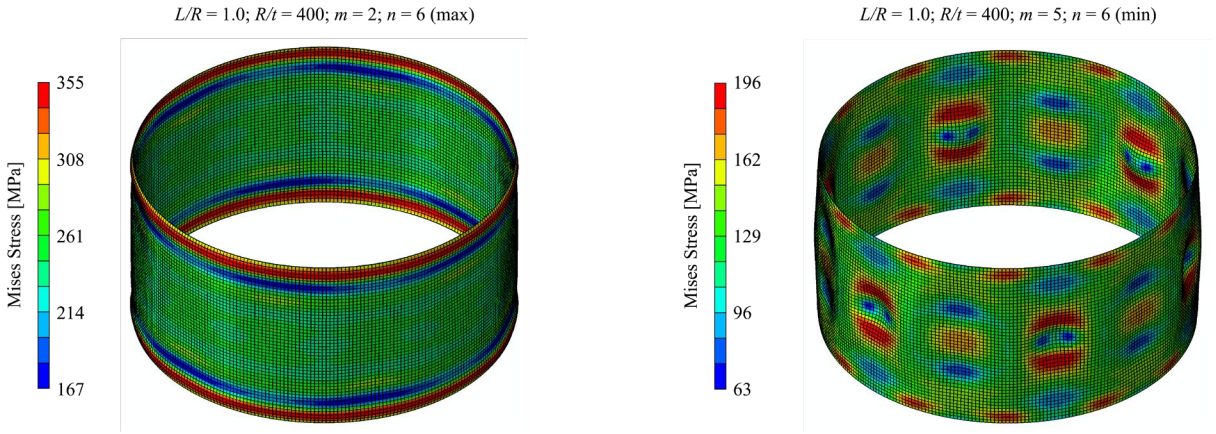

Figure 9(b). Typical collapse modes of long slender cylindrical shell

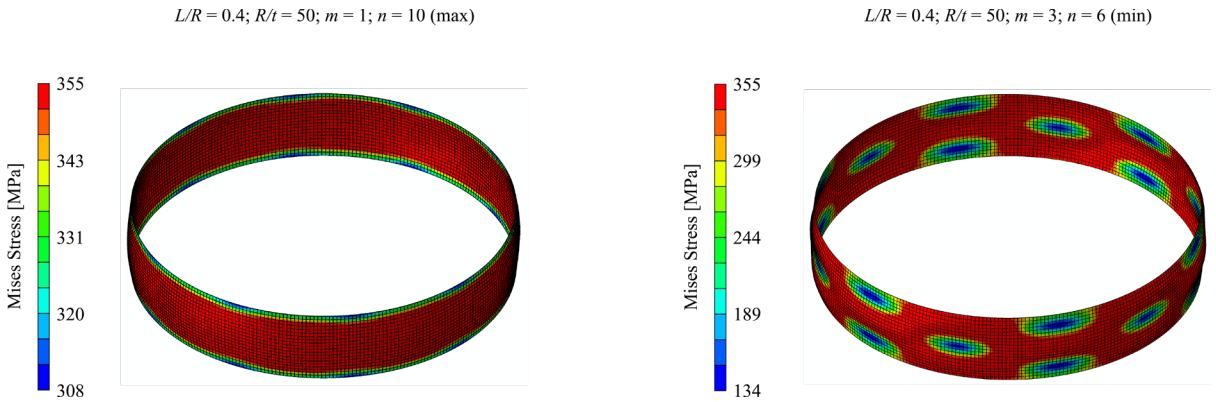

Figure 9(c). Typical collapse modes of short stocky cylindrical shell

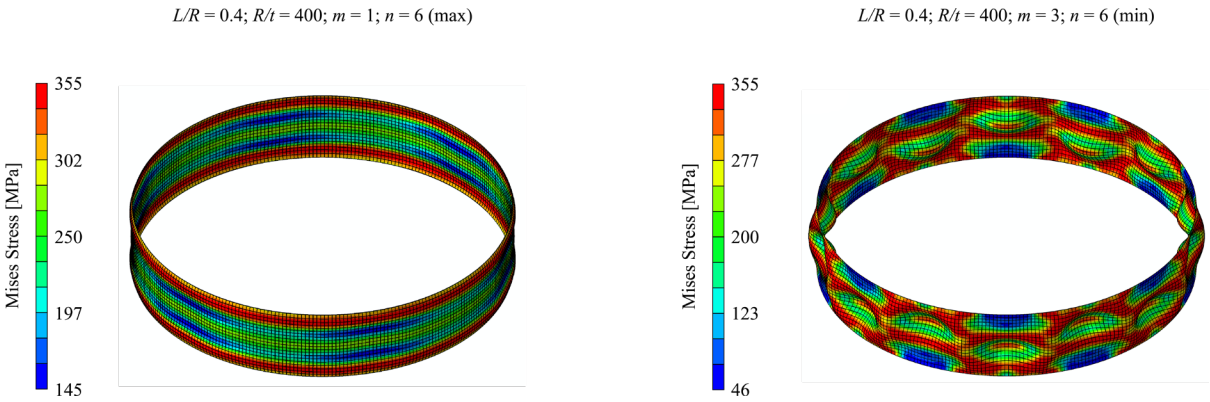

Figure 9(d). Typical collapse modes of short slender cylindrical shell

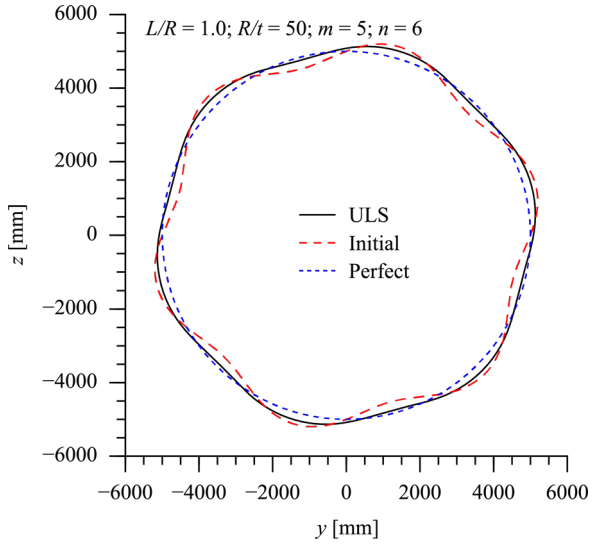

Figure 10(a). Example comparison of the circumferential deflection (consistent pattern between initial and collapse states)

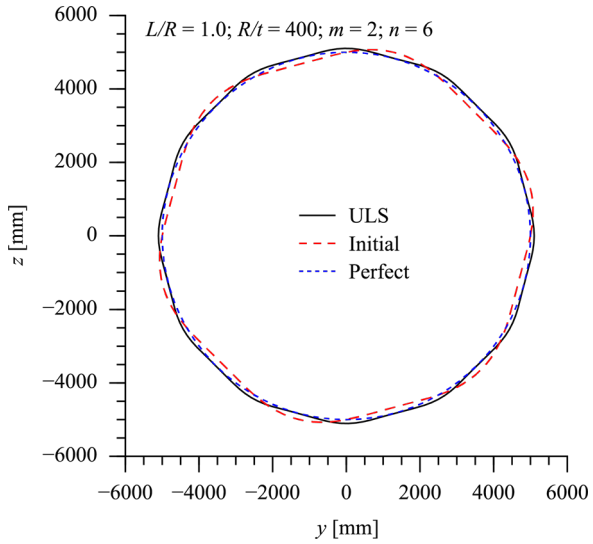

Figure 10(b). Example comparison of the circumferential deflection (inconsistent pattern between initial and collapse states)

5.2 Effects of Imperfection Shapes

The computed ultimate strength of the unstiffened cylindrical shell is shown in **Figures 11 and 12**, as a function of the full-wave number in the circumferential direction (n) and the half-wave number in the longitudinal direction (m), respectively.

It is clear that the stocky cylindrical shell structures are considerably less sensitive to the variation in imperfection shapes. Conversely, higher sensitivity to the imperfection shapes is found on slender cylindrical shell models.

A larger half-wave number in the circumferential direction generally results in a strength reduction of the structures. Nevertheless, there is also an increase of the ultimate strength in some cases, i.e. stocky cylindrical shell and long slender cylindrical shell with m = 4 and 5. This observation may be supported by the analytical finding in **[35]**, where a wavy shape was exploited to give an optimal buckling strength of cylindrical shell under axial compression. However, this increase in the buckling and ultimate strength, at least for the present case study modes, appears to be relatively small.

In terms of the influence of half-wave number in the longitudinal direction, a higher-order longitudinal deflection leads to a smaller ultimate strength of the unstiffened cylindrical shell, in particular the slender shell structures. This is generally in agreement with the insights developed in flat plates **[36]**. Comparing **Figures 11** and **12**, it may be noticed that the ultimate strength of cylindrical shell under axial compression is more sensitive to the longitudinal deflection shape.

The ultimate strength of a long slender cylindrical shell combined with rotational-symmetric imperfection is shown in **Figure 13**. Consistent with the above observation, the ultimate strength of the shell structure reduces with the increase in longitudinal half-wave number. However, the reduction rate appears to be lower comparing with that in **Figure 12(b)**. Moreover, the collapse modes at ULS in these scenarios preserve the initial imperfection pattern as presented in **Figure 14**, which is of a distinct difference compared with the deformation localisation observed in the non-rotational-symmetric initial imperfection.

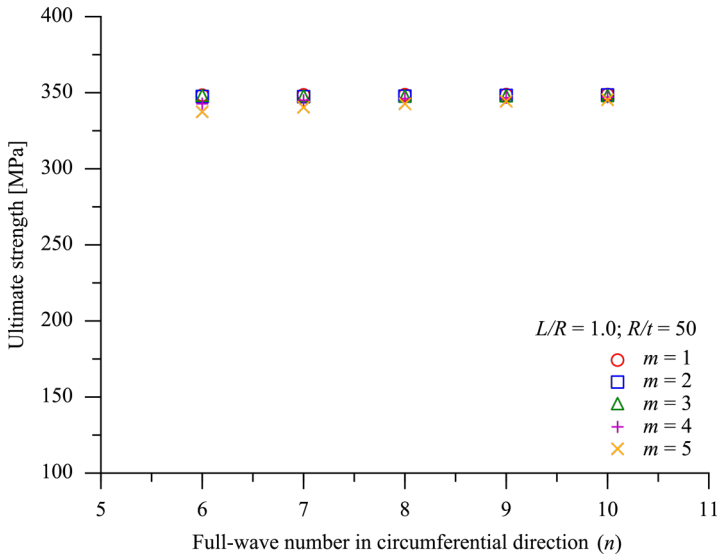

Figure 11(a). The ultimate strength of long stocky cylindrical shell as a function of the full-wave number in the circumferential direction (n)

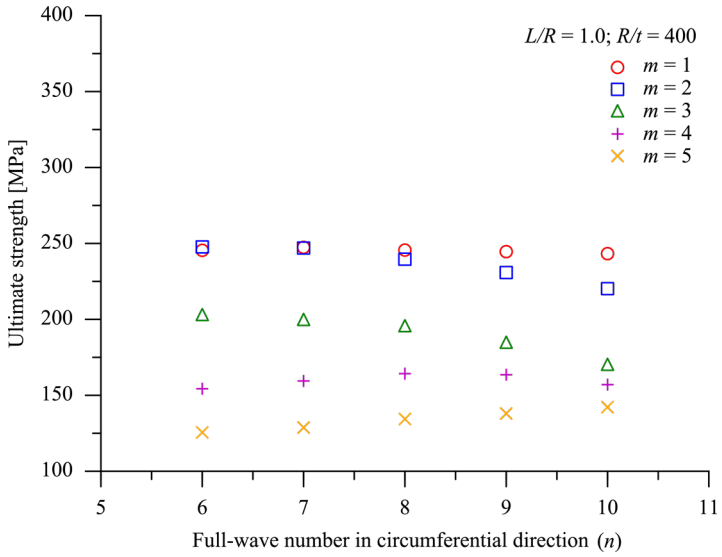

Figure 11(b). The ultimate strength of long slender cylindrical shell as a function of the full-wave number in the circumferential direction (n)

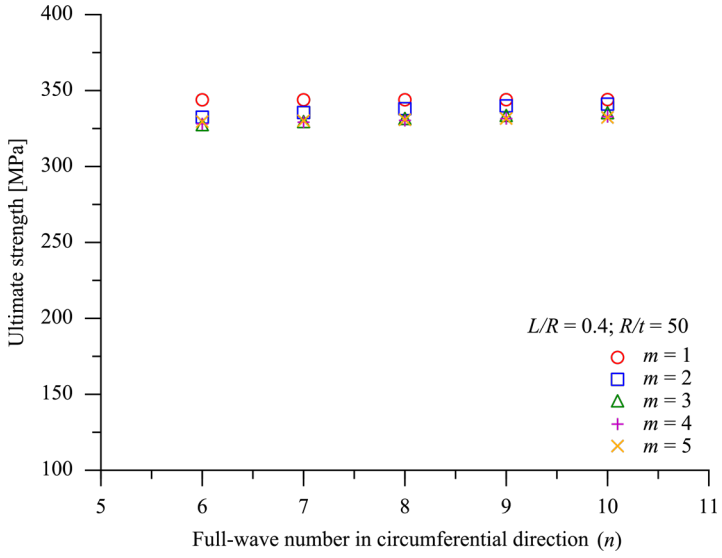

Figure 11(c). The ultimate strength of short stocky cylindrical shell as a function of the full-wave number in the circumferential direction (n)

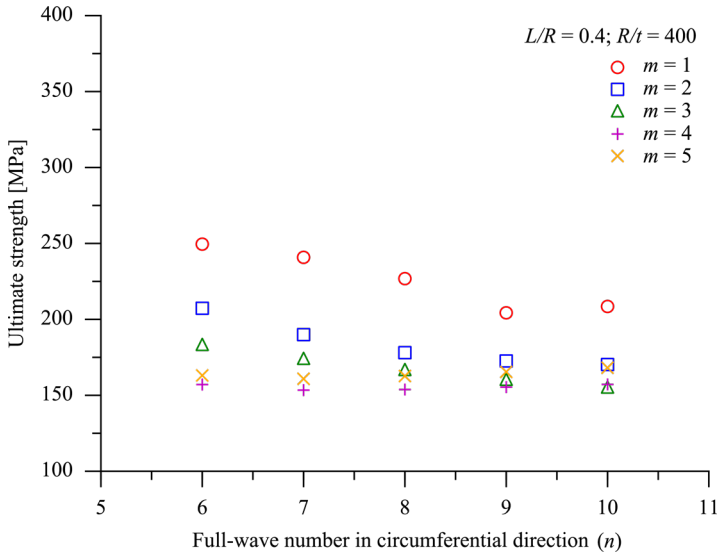

Figure 11(d). The ultimate strength of short slender cylindrical shell as a function of the full-wave number in the circumferential direction (n)

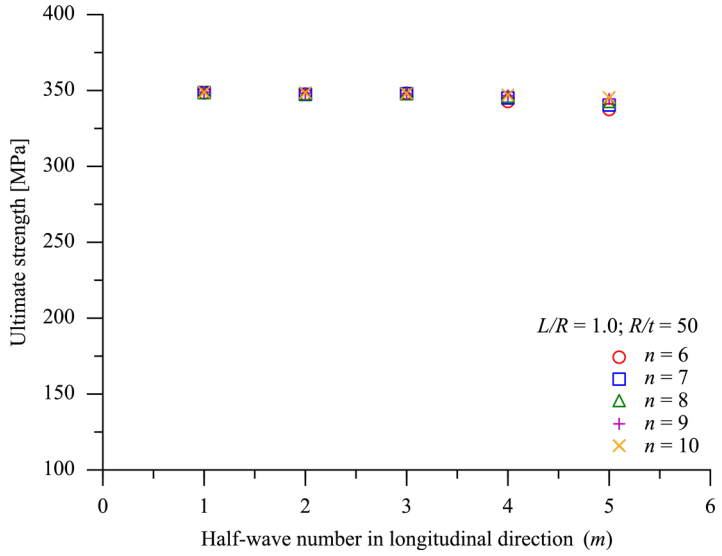

Figure 12(a). The ultimate strength of unstiffened cylindrical shell as a function of the half-wave number in the longitudinal direction (m)

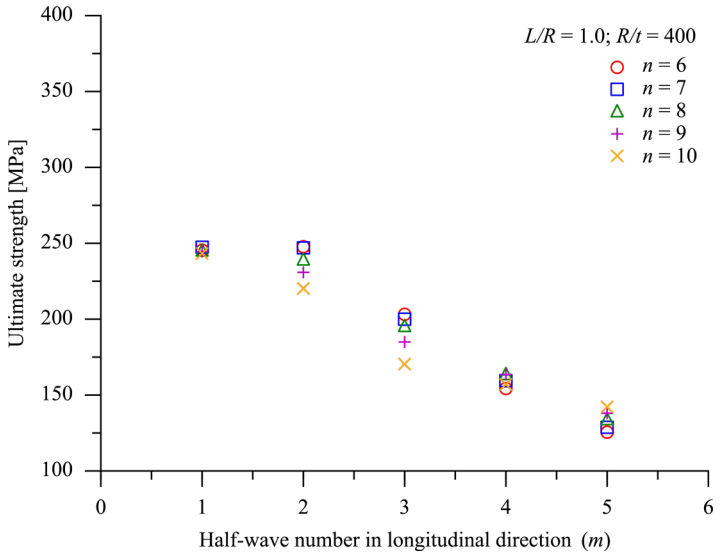

Figure 12(b). The ultimate strength of unstiffened cylindrical shell as a function of the half-wave number in the longitudinal direction (m)

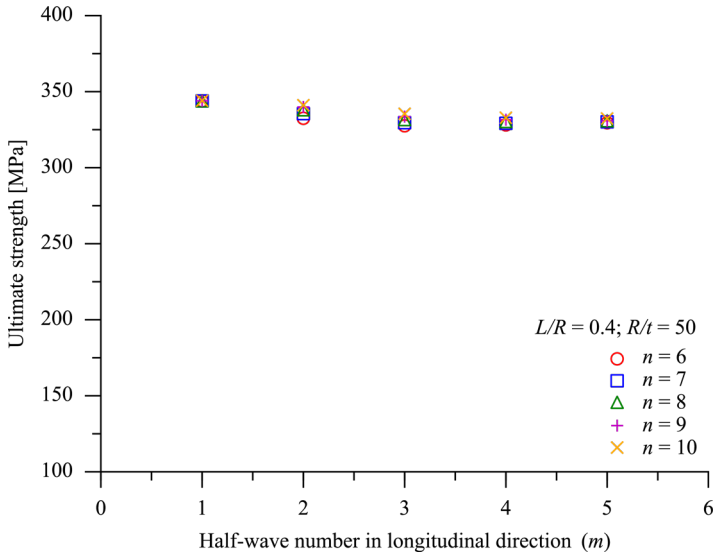

Figure 12(c). The ultimate strength of unstiffened cylindrical shell as a function of the half-wave number in the longitudinal direction (m)

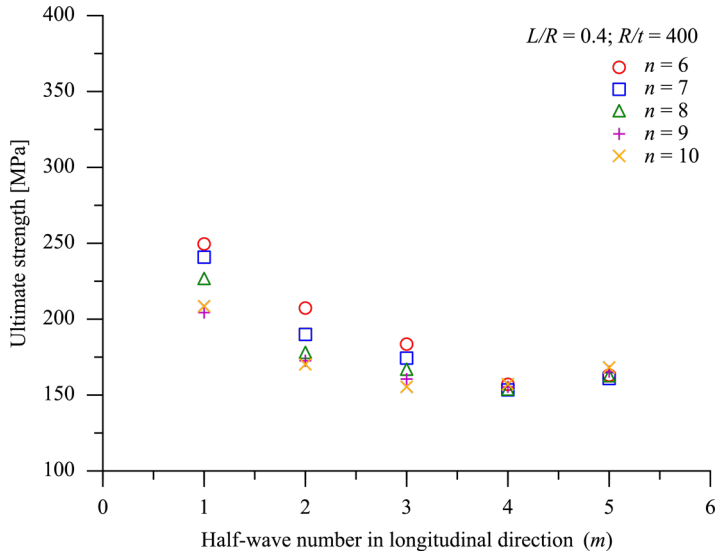

Figure 12(d). The ultimate strength of unstiffened cylindrical shell as a function of the half-wave number in the longitudinal direction (m)

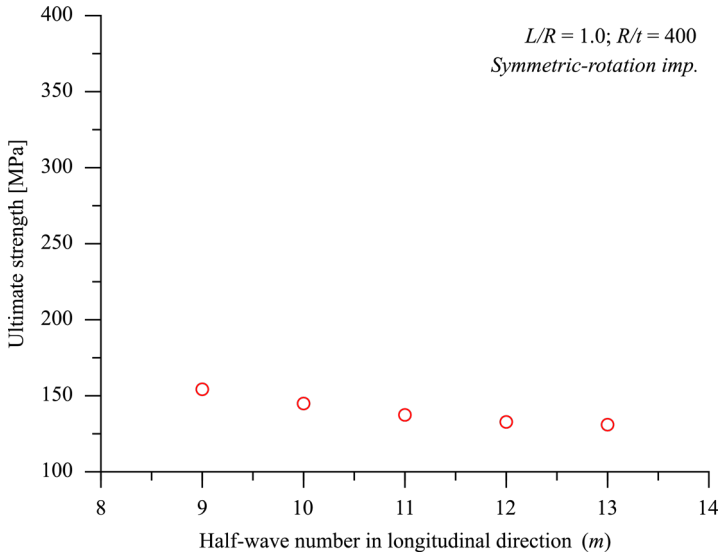

Figure 13. The ultimate strength of long slender cylindrical shell with rotational-symmetric imperfection

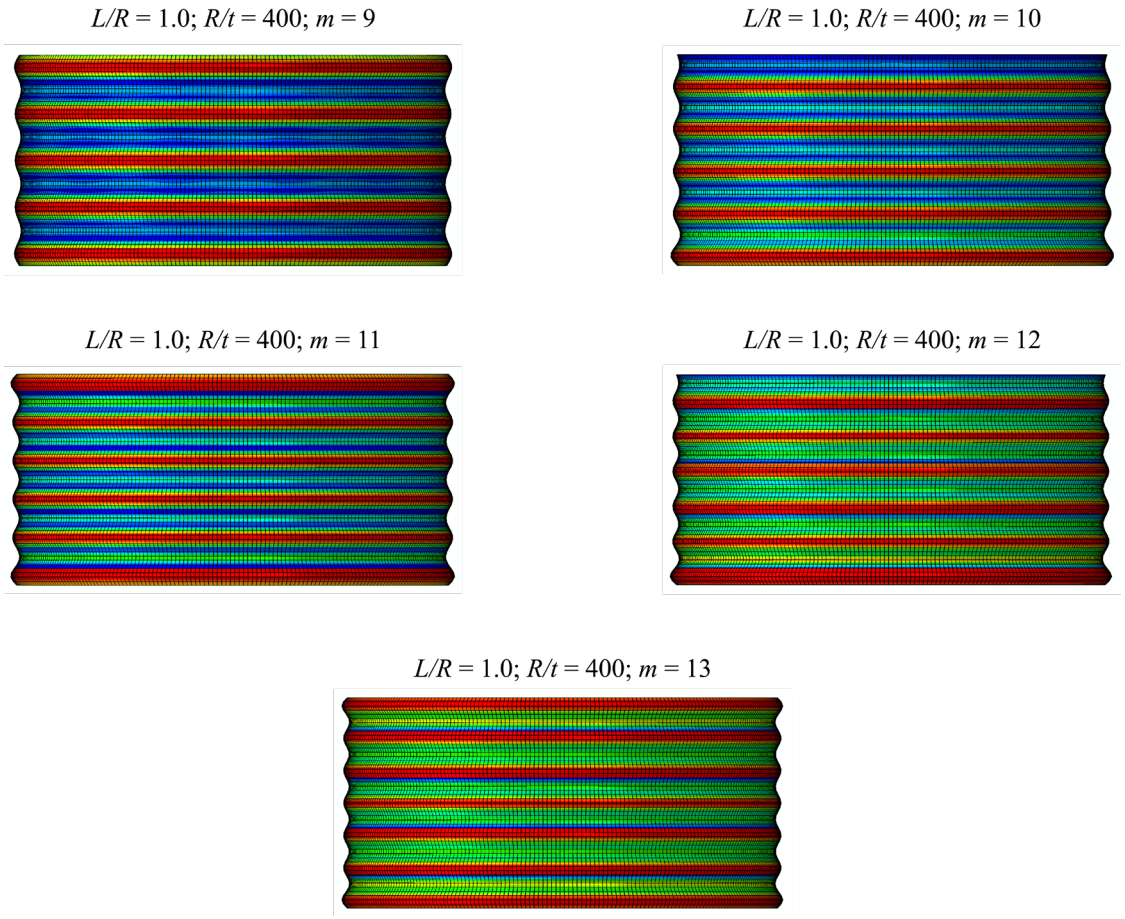

Figure 14. Collapse modes of long slender cylindrical shells with rotational-symmetric imperfections

6. Comparison between Numerical Prediction and Code Formulae

A comparison of the cylindrical shell's ultimate strength predicted by finite element analysis and code-based formulae (i.e., DNV, ABS, API and Eurocode given in section 2) is completed for the cylindrical shell with $L/R = 0.4$ and $R/t = 50$, 100, 200, 400. Likewise, the radius of all models is fixed to be 5000mm. The length and thickness are parametrically varied according to the dimensionless ratio. In terms of the material property, the yield strength and elastic modulus in all calculations are 355 MPa and 207 GPa, respectively. Only one length-to-radius ratio is tested because of the insensitivity of the code formula to the length of cylindrical shells. Note that the first-order linear eigenmode is used for modelling the initial geometric imperfection shape for each cylindrical shell. The comparisons between the numerical results and code formula prediction are

shown in **Figure 15** and **Figure 16**. The former is a comparison on the characteristic/critical buckling strength, while the latter is the comparison of design buckling. In design codes, the characteristic/critical buckling strength is the theoretical capacity prediction. The design buckling strength is a factored value of the former, given in the limit state equation and usually taking into account of a partial safety factor.

As shown in the comparison, there is a large deviation between different code formulae. The prediction by API is the most optimistic one (both characteristic/critical and design values). Eurocode 3 ($Q = 16$) has the most conservative characteristic/critical buckling strength prediction, while DNV gives the most conservative design buckling strength. As compared with the present FE results, all of the code formulae appear to be overly conservative. In the case of characteristic or critical buckling strength, the API is close to the numerical prediction. However, when it comes to the design buckling strength, it is underestimated by all code formulae. The ratios between the characteristic/critical and design buckling strength in different codes are illustrated in **Figure 17**. It can be seen that the partial safety factor applied to the design buckling strength is up to 1.4 in some cases in the DNV formula. In future research, it might be useful to re-visit these partial safety factors, especially if one wants to apply these design codes to offshore wind structures. These design codes were initially developed for the oil and gas industry. The consequence of structural failure is probably much more severe due to the manned operation and hydrocarbon production. Conversely, the operation is usually remotely controlled in the offshore wind industry, and there is no risk associated with hydrocarbon production. Hence, the consequence of failure may substantially differ, which suggests some of these rather conservative safety factors can relieve to a certain extent.

Nevertheless, it should be noted that the above discussion is based upon the assumption of first-order eigenmode imperfection with maximum magnitude defined in Section 3.3. More concrete conclusions shall be developed, once sufficient full-scale measurement of the initial imperfection of cylindrical shells used in maritime sector is available.

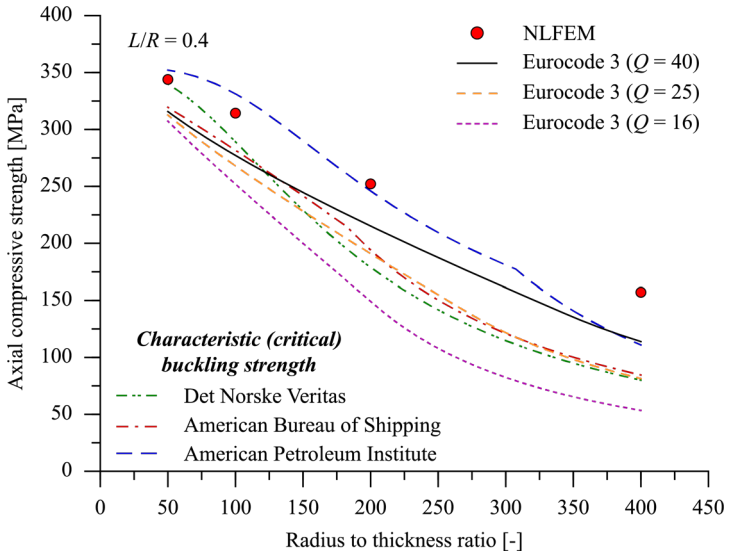

Figure 15. Comparison of numerical results and code formula prediction (characteristic/critical buckling strength)

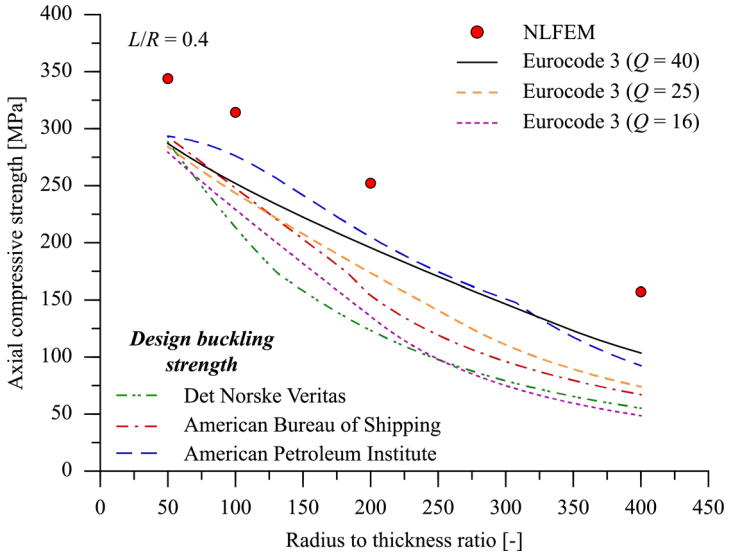

Figure 16. Comparison of numerical results and code formula prediction (design buckling strength)

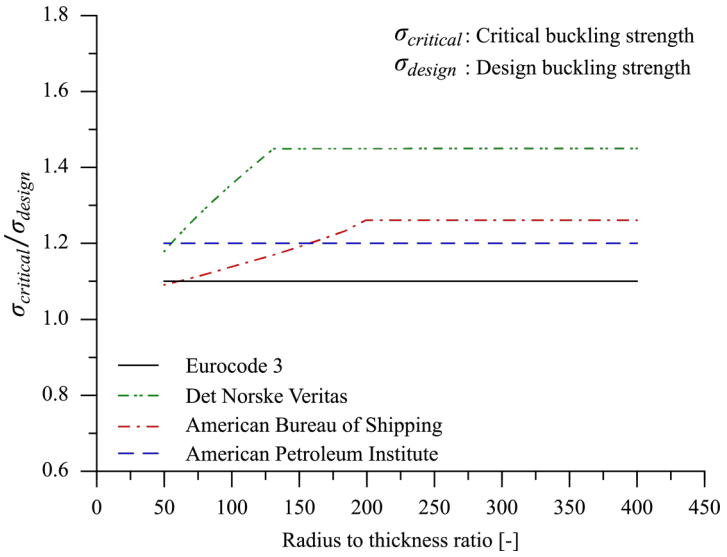

Figure 17. Ratios between characteristic/critical and design buckling strength in different code formulae

7. Concluding Remarks and Recommendations

This study performed a parametric investigation using the nonlinear finite element method on the ultimate strength characteristics of unstiffened cylindrical shell structures under axial compression. The emphasis is placed on the sensitivity of ultimate strength to initial geometric imperfection. Cylindrical shells with different length-to-radius ratios and radius-to-thickness ratios are analysed. From this study, the following conclusions may be drawn:

- The ultimate collapse of stocky cylindrical shells structures is dominated by gross yielding and is, therefore, less sensitive to the initial geometric imperfection.
- The ultimate collapse of slender cylindrical shell structures is triggered by elastic or elastoplastic buckling and is therefore highly sensitive to the initial geometric imperfection.
- Different numbers of full-wave in the circumferential direction and half-wave in the longitudinal direction of the initial geometric imperfection have considerable effects on the ultimate strength of cylindrical shells. The longitudinal deflection shape is generally more influential than the deflection shape in the circumferential direction.

- The ultimate capacity of cylindrical shell appears to be more sensitive to the non-rotational-symmetric imperfection shape, whereas the sensitivity to rotational-symmetric imperfection pattern is lower.
- There is a considerable deviation between DNV, ABS, API and Eurocode 3 on the prediction of cylindrical shell axial compressive strength. In comparison with the present numerical data, these formulae, some of which are originally developed for the oil and gas industry, appear to be conservative.

The present study provides valuable insights for the ultimate limit state analysis of cylindrical shell structures under axial compression. This is a relevant topic for the safety design of offshore wind turbine structures. Nevertheless, understanding of the structural response of cylindrical shells operating in a marine environment is still insufficient. In order to improve the current state-of-the-art, the following should be addressed in future research:

- A campaign of full-scale measurement of the initial imperfection of cylindrical shells used in wind turbine structures is recommended, as both geometric imperfection shape and magnitude are currently lack of precise guidance.
- Based upon the measurement data, deterministic and probabilistic models of geometric imperfection shall be developed. Relevant study and insights developed from ship-type flat plates may refer to [37].
- The collapse behaviour of cylindrical shells under combined loads, such as combined compression, bending moment and hydrostatic pressure, should be thoroughly investigated.
- Improved design formula to predict the ultimate capacity of cylindrical shell structures is needed. The procedure to develop these formulae may refer to [38-40].
- More physical testing will be helpful for benchmarking the analytical modelling and numerical simulation.

References

[1]. Shafiee, M., Brennan, F., Espinosa, I.A, 2016. A parametric whole life cost model for offshore wind farms. The International Journal of Life Cycle Assessment, 21(7), 961-975.

[2]. Lozano-Minguez, E., Kolios, A.J., Brennan, F.P., 2011. Multi-criteria assessment of offshore wind turbine support structures. Renewable Energy, 36(11), 2831-2837.

[3]. Sunday, K., Brennan, F., 2021. A review of offshore wind monopiles structural design achievements and challenges. Ocean Engineering, 235, 109409.

[4]. Paik, J.K., 2020. Advanced structural safety studies: with extreme conditions and accidents, Springer.

[5]. Paik, J.K., 2018. Ultimate limit state analysis and design of plated structures, Wiley Online Library.

[6]. Jia, J.B., Paik, J.K., 2018. Engineering Dynamics and Vibrations, CRC Press.

[7]. Li. C.B., Choung, J., 2021. A new method of predicting hotspot stresses for longitudinal attachments with reduced element sensitivities. International Journal of Naval Architecture and Ocean Engineering, 13, 379-395.

[8]. Kim, D.K., Incecik, A., Choi, H.S., Wong, E.W.C., Yu, S.Y., Park, K.S., 2018. A simplified method to predict fatigue damage of offshore riser subjected to vortex-induced vibration by adopting current index concept, Ocean Engineering, 157, 401-411.

[9]. Yu, Z.L., Amdahl, J., Sha, Y., 2018. Large inelastic deformation resistance of stiffened panels subjected to lateral loading, Marine Structures 59, 342-367.

[10]. Kim, D.K., Kim, B.J., Seo, J.W., Kim, H.B., Zhang, X.M., Paik, J.K., 2014. Time-dependent residual ultimate longitudinal strength-groundingdamage index (R-D) diagram. Ocean Engineering, 76, 163-171.

[11]. Yeter, B., Garbatov, Y., Guedes Soares, C., 2019. Numerical and experimental study of the ultimate strength of a monopile structure. Engineering Structures, 194, 290-299.

[12]. Li, S., Kim, D.K., Benson, S., 2021. The influence of residual stress on the ultimate strength of longitudinally compressed stiffened panels. Ocean Engineering, 231, 108839.

[13]. Ringsberg, J.W., Darie, I., Nahshon, K., Shilling, G., Vaz, M.A., Benson, S., Brubak, L. Feng, G.Q., Fujikubo, M., Gaiotti, M., Hu, Z.Q., Jang, B.S., Paik, J.K., Slagstad, M., Tabri,

K., Wang, Y.K., Wiegard, B., Yanagihara, D., 2021. The ISSC 2022 committee III.1-Ultimate strength bench-mark study on the ultimate limit state analysis of a stiffened platestructure subjected to uniaxial compressive loads, Marine Structures, 79, 103026.

[14]. Li, S., Kim, D.K., Benson, S., 2021. A probabilistic approach to assess the computational uncertainty of ultimate strength of hull girders, Reliability Engineering & System Safety, 107688.

[15]. Kim, S.E., Kim, C.S., 2002. Buckling strength of the cylindrical shell and tank subjected to axially compressive loads. Thin-Walled Structures, 40(4), 329-353.

[16]. Shiomitsu, D., Yanagihara, D. 2021. Estimation of ultimate strength of ring-stiffened cylindrical shells under external pressure with local shell buckling or torsional buckling of stiffeners. Thin-Walled Structures, 161, 107416.

[17]. Shiomitsu, D., Yanagihara, D. 2020. Elastic local shell and stiffener-tripping buckling strength of ring-stiffened cylindrical shells under external pressure. Thin-Walled Structures, 148, 106622.

[18]. Cho, S.R., Muttaqie, T., Do, Q.T., So, H.Y., Sohn, J.M, 2018. Ultimate strength formulation considering failure mode interactions of ring-stiffened cylinders subjected to hydrostatic pressure. Ocean Engineering, 161, 242-256.

[19]. Graham, D., 2007. Predicting the collapse of externally pressurised ring-stiffened cylinders using finite element analysis. Marine Structures, 20, 202-217.

[20]. Ghazijahani, T.G., Jiao, H., Holloway, D., 2014. An experimental study on externally pressurized stiffened and thickened cylindrical shells. Thin-Walled Structures, 85, 359-366.

[21]. Cho, S.R, Do, Q.T., Shin, H.K., 2017. Residual strength of damaged ring-stiffened cylinders subjected to external hydrostatic pressure. Marine Structures, 56, 186-205.

[22]. Ghazijahani, T.G., Showkati, H., 2013. Experiments on cylindrical shells under pure bending and external pressure. Journal of Constructional Steel Research, 88, 109-122.

[23]. Cerik, B.C., 2015. Ultimate strength of locally damaged steel stiffened cylinders under axial compression. Thin-Walled Structures, 95, 138-151.

[24]. Ghazijahani, T.G., Jiao, H., Holloway, D., 2014. Experimental study on damaged cylindrical shells under compression. Thin-Walled Structures, 80, 13-21.

[25]. Weaver, P.M., 2000. Design of laminated composite cylindrical shells under axial compression. Composite Part B: Engineering, 31(8), 669-679.

[26]. Wang, B., W., Zhu, S.Y., Hao, P., Bi, X.J., Du, K.F., Chen, B.Q., Ma, X.T., Chao, Y.J. 2018. Buckling of quasi-perfect cylindrical shell under axial compression: A combined experimental and numerical investigation. International Journal of Solids and Structures, 130-131, 232-247

[27]. Schmidt, H., Winterstetter, T.A., 1999. Buckling Interaction Strength of Cylindrical Steel Shells Under Axial Compression and Torsion. In Proceeding: The 2nd International Conference on Advances in Steel Structures, Hong Kong, China.

[28]. Pal'chevskii, A.S., 1966. On a mode of buckling of circular cylindrical shells under axial compression. Soviet Applied Mechanics, 2, 80-81.

[29]. Cho, Y.S., Oh, D.H., Paik, J.K., 2019. An empirical formula for predicting the collapse strength of composite cylindrical-shell structures under external pressure loads. Ocean Engineering, 172, 191-198.

[30]. DNVGL, 2018. Buckling strength of shells. DNVGL-RP-C202.

[31]. ABS, 2016. Guide for buckling and ultimate strength assessment for offshore structures (LRFD version).

[32]. API, 2004. Bulletin on stability design of cylindrical shells.

[33]. Eurocode 3, 2006. Design of steel structures – Part 1-6: Strength and stability of shell structures.

[34]. Friedrich, L., Schmid-Fuertes, T.A., UweSchröder, K., 2015. Comparison of theoretical approaches to account for geometrical imperfections of unstiffened isotropic thin walled cylindrical shell structures under axial compression. Thin-Walled Structures, 92, 1-9.

[35]. Ning, X., Pellegrino, S., 2015. Imperfection-insensitive axially loaded thin cylindrical shells. International Journal of Solids and Structures, 62, 39-51.

[36]. Gordo, J.M., 2015. Effect of initial imperfections on the strength of restrained plates. Journal of Offshore Mechanics and Arctic Engineering, 137(5), 051401.

[37]. Georgiadis, D.G., Samuelides, M.S., 2021. Stochastic geometric imperfections of plate elements and their impact on the probabilistic ultimate strength assessment of plates and hull girders, 76, 102920.

[38]. Kim, D.K., Lim, H.L., Kim, M.S., Hwang, O.J., Park, K.S., 2017. An empirical formulation for predicting the ultimate strength of stiffened panels subjected to longitudinal compression, Ocean Engineering 140, 270-280.

[39]. Kim, D.K., Lim, H.L., Yu, S.Y., 2019. Ultimate strength prediction of T-bar stiffened panel under longitudinal compression by data processing: A refined empirical formulation, Ocean Engineering 192, 106522.

[40]. Kim, D.K., Yu, S.Y., Lim, H.L., Cho, N.K., 2020. Ultimate compressive strength of stiffened panel: An empirical formulation for flat-bar type. Journal of Marine Science and Engineering 8, 605.